



Ultrafast photoinduced deligation and ligation dynamics: DCM in micelle and micelle-enzyme complex

Rupa Sarkar, Ajay Kumar Shaw, Manoranjan Ghosh, Samir Kumar Pal *

Unit for Nano Science and Technology, S.N. Bose National Centre for Basic Sciences, Block JD, Sector III, Salt Lake, Kolkata 700 098, India

Received 30 July 2005; received in revised form 28 December 2005; accepted 2 January 2006

Abstract

We report studies on diffusion controlled deligation and ligation dynamics of a probe ligand 4-(dicyanomethylene)-2-methyl-6-(*p*-dimethylamino-styryl) 4H-pyran (DCM) with cationic cetyltrimethylammonium bromide (CTAB) micelles. In order to investigate the effect of spatial heterogeneity on the dynamics we study the DCM labeled micelle upon complexation with an enzyme α -chymotrypsin (CHT). The variation of fluorescence line-width ($\Gamma(t)$) of DCM in the complex and also in the micelle indicates the diffusion dynamics of DCM through various environments of different polarities. The temporal behavior of $\Gamma(t)$ reveals that at 50 mM CTAB concentration the excited DCM traverses 6.5 Å distance from the surface of a host micelle (deligation) before entering to a stern layer of another adjacent micelle (ligation). From neutron scattering experiment the distance 6.5 Å is found to be the thickness of a stern layer of CTAB micelle. No indication of ligation has been found at 2 mM CTAB concentration as the intermicellar distance is estimated to be very large (416 Å) compared to the previous case. The dynamical behavior of $\Gamma(t)$ is also indicative of significantly slower diffusion of the ligand molecules (DCM) at the surface of the micelle in presence and absence of the enzyme compared to that in the bulk buffer. We have also studied the dynamics of solvation and local geometrical restriction on the probe DCM at the micellar surface with and without CHT. With picosecond time resolution, we found time constants of the solvation relaxation processes of the DCM labeled enzyme-micelle complex to be 230 ps (45%) and 870 ps (55%), which were comparable to those of the micelle without the enzyme. The time dependent anisotropy revealing local orientational motions of the probe in the complex was also found to be similar to that of DCM at the micellar surface in absence of CHT. These studies attempt to link the dynamical features for insight into the ligand mediated intercellular communication and the biological function of the enzyme α -chymotrypsin upon complexation with the CTAB micelle.

© 2006 Elsevier B.V. All rights reserved.

Keywords: Deligation and ligation dynamics; Solvation; DCM; Temporal FWHM; Anisotropy; Picosecond resolved fluorescence transients; CTAB micelle

1. Introduction

Intercellular communication is extremely important in the growth of living cells and tissues [1,2]. Tissues are comprised of *functional units* such as nephron in the kidney and the villi in the small intestine. The functional units contain many different cell types that continuously communicate with one another through a variety of mechanisms. A key mode of communication is the release of soluble cyto- and chemokines. These signals lead to the induction

of organogenic processes, such as cell proliferation, differentiation and motion [1–3]. A theoretical work [3] using solitary cell model estimated effective communication distance over which a single cell can meaningfully propagate a ligand (cyto/chemokines)-mediated signal to be $\sim 25 \mu\text{m}$ and the communication within this domain takes place in 10–30 min. The experimental observations [4] were in agreement with the estimated values. An important family of epithelial patterning mechanisms relies on secreted chemical signals. Typically a ligand released by a group of cells interacts with the extracellular matrix and cell surface receptors as it spreads through the tissue. A recent theoretical work [5] on the intercellular communication in

* Corresponding author. Tel.: +91 33 2335 578; fax: +91 33 2335 3477.
 E-mail address: skpal@bose.res.in (S.K. Pal).

epithelial layers derived cell-to-cell coupling coefficients as a function of geometric, cellular and molecular parameters of the ligand transport mechanisms. A rapid decay in the coupling coefficients as a function of intercellular distance suggested from the model [5] was in the line with the conclusions of experimental studies [6]. Fig. 1 is a schematic representation of ligand-mediated intercellular communication. As shown in Fig. 1 and mentioned in the theoretical model [5] the efficiency of intercellular communication decays with the effective distance between two cells (secreting and receiving).

In this work we use an organic laser dye 4-(dicyanomethylene)-2-methyl-6-(*p*-dimethylamino-styryl) 4H-pyran (DCM) and a micelle as model systems of the ligand and the cell respectively. The micellar organizations have been used as mimic-systems in order to represent biological macromolecules [7]. The micelle is cationic in nature and is made of cationic surfactant cetyltrimethylammonium bromide (CTAB). Small angle neutron scattering experiments [8–10] on the aqueous micellar solution of CTAB reveal the diameter of the micelle to be 10 nm. The thickness of the stern layer, which is made of dynamically rigid water molecules and counter ions (bromide) of the micelle, has also been found to be 1 nm [8–10]. The laser dye DCM, a well known spectroscopic probe [11–14] is completely insoluble in water and has selective binding affinity to the CTAB micellar surface. The dye is completely hydrophobic (nonpolar) in the ground state. However, UV excitation increases dipole moment of the probe making it polar and hence increases its hydrophilicity in the excited state [13,14]. Thus the excited DCM diffuses from the micellar surface (relatively nonpolar) towards polar bulk water phase revealing a fluorescence emission signature of the excursion through multiple environments in the excited state.

In order to study the effect of environmental heterogeneity on the ligand probe (DCM), we have also investigated the dynamics of the ligand in the micelle upon complexation with an enzyme. The enzyme bovine pancreatic α -chymo-

trypsin (CHT) is in a class of digestive enzymes of molecular weight 25 kD. In a recent study [15] it has been shown that CHT makes complex with the micelle and the complexation leads to superactivity of the enzyme compared to that of free CHT in buffer solution. However, our previous study [16] on the complex by using a different substrate molecule reveals seven times retarded activity of the enzyme compared to that in the buffer solution. In the present study, by observing the picosecond to nanosecond dynamics of population and polarization analyzed anisotropy of the ligand molecules for the micelle and the enzyme-micelle complex, we elucidate the nature of local solvation and spatial geometrical restriction on the probes. The efficacy of the communication between two micelles has been investigated by the ligation and deligation dynamics of the ligand by measuring picosecond resolved line-width of the ligand fluorescence indicative of the diffusion of the excited probe molecules through various environments of different polarities. In order to show the effect of intermicellar distance on the efficacy of ligation, the concentration of the micelle (inversely proportional to the intermicellar distance) has been varied and observed a strong dependency of the efficacy on the distance between two micelles.

2. Materials and methods

The enzyme CHT from bovine pancreas was purchased from Sigma, CTAB from Fluka and DCM was from Exciton. All samples were used as received without further purifications. Aqueous solutions were prepared in phosphate buffer (0.1 M, pH 7). The DCM-micelle complexes were prepared by mixing of DCM (35 μ M) with CTAB (50 mM and 2 mM) in the neutral buffer solution and the mixture was kept at room temperature for 3 h. The enzyme-micelle complex was prepared by mixing 1 mM CHT with 0.942 mM DCM-labeled micelle ([CTAB] = 50 mM) and stirring the solution for 3 h (enzyme:micelle \approx 1:1).

Steady-state absorption and emission were measured with Shimadzu Model UV-2450 spectrophotometer and Jobin Yvon Model Fluoromax-3 fluorimeter respectively. All transients were taken by using commercially available (IBH, UK) picosecond-resolved time correlated single photon counting (TCSPC) setup (instrument response function (IRF) of \sim 220 ps). The picosecond excitation pulse from the diode laser was used at 405 nm. The fluorescence from the sample was detected by a photomultiplier after dispersion through a double grating monochromator. For all transients the polarizer in the emission side was adjusted to be at 54.7° (magic angle) with respect to the polarization axis of excitation beam.

Upon excitation of the probe ligand (DCM) using a picosecond laser pulse a significant dipole moment is generated in the ligand and hence the polar solvent molecules at $t = 0$ find themselves in a relatively high-energy configuration [17]. Subsequently, as shown in the upper panel of Fig. 2, the solvent molecules begin to move and rearrange

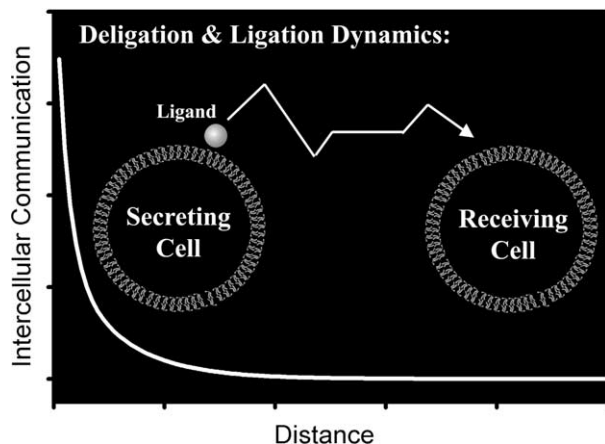


Fig. 1. A schematic representation of diffusion controlled ligand mediated intercellular communication. The efficiency of the communication decreases with the effective intercellular separation.

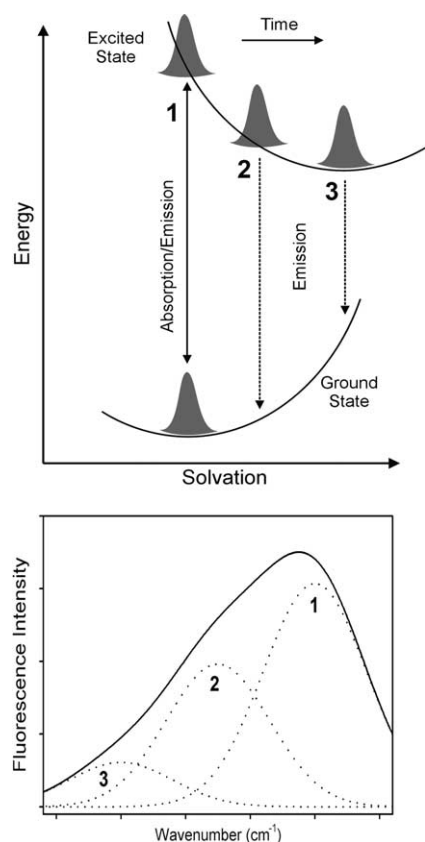


Fig. 2. *Upper.* A schematic representation of spectral diffusion on the excited state potential surface. Emission spectra 1, 2 and 3 reflect the evolution of the solvation free-energies along the solvation coordinate. *Lower.* Time integrated fluorescence emission spectrum. The solid line is convolution of three representative emission spectra 1, 2 and 3 (dotted lines) that results from solvation of the probe ligand.

themselves to reach their new equilibrium positions. The nuclear motion involved can be broadly classified into rotational and translational motions. The shift in the ligand's emission frequency (peak), which accompanies the solvent relaxation is then a measure of the dynamics of solvation. The time integrated fluorescence emission spectrum (steady-state) of various solvated states is shown in the lower panel of Fig. 2. To construct time-resolved emission spectra (TRES) after the excitation pulse, we adopted the method of the reference [17]. For every sample solution, the fluorescence transients were measured as a function of the detected wavelength in the range of 540–740 nm.

The observed fluorescence transients were fitted using a nonlinear least squares fitting procedure (software SCIEN-TIST™) to a function comprising of the convolution of the instrument response function (IRF) with a sum of exponentials. The purpose of this fitting is to obtain the decays in an analytic form suitable for further data analysis. For each transient detected at a particular wavelength, was normalized by using the steady-state spectrum. The resulting time-resolved spectra were fitted with a Lognormal shape function to estimate the spectrum maximum $\nu(t)$. The temporal Stokes shift can be represented by the time dependence of the fit. By following the time-resolved emis-

sion, we constructed the solvation correlation function, $C(t) = [\nu(t) - \nu(\infty)]/[\nu(0) - \nu(\infty)]$, where $\nu(0)$, $\nu(t)$ and $\nu(\infty)$, denote the observed emission energies (in wavenumbers) at time 0, t and ∞ , respectively. For anisotropy measurements, emission polarization was adjusted to be parallel or perpendicular to that of the excitation and the anisotropy is defined as $r(t) = [I_{\text{para}} - G \cdot I_{\text{perp}}]/[I_{\text{para}} + 2 \cdot G \cdot I_{\text{perp}}]$. The magnitude of G , the grating factor of the emission monochromator of the TCSPC system was found by using a coumarin dye in methanol and following long-time tail matching technique [18] to be 2.1.

Fig. 3 is a schematic representation of the effect of excited state diffusion of a probe molecule through various environments of different polarities on TRES. The upper panel (left) shows distribution of the probe molecules in a microheterogeneous environment, where polarity of environment-1 is lower than environment-2, which is relatively nonpolar compared to that of environment-3. The characteristic emission spectra of the probes in the three different environments (solvatochromism) are also shown in the right side of the upper panel; the fluorescence emission maximum in the nonpolar environment is in the blue side compared to that in the polar environment. The overall

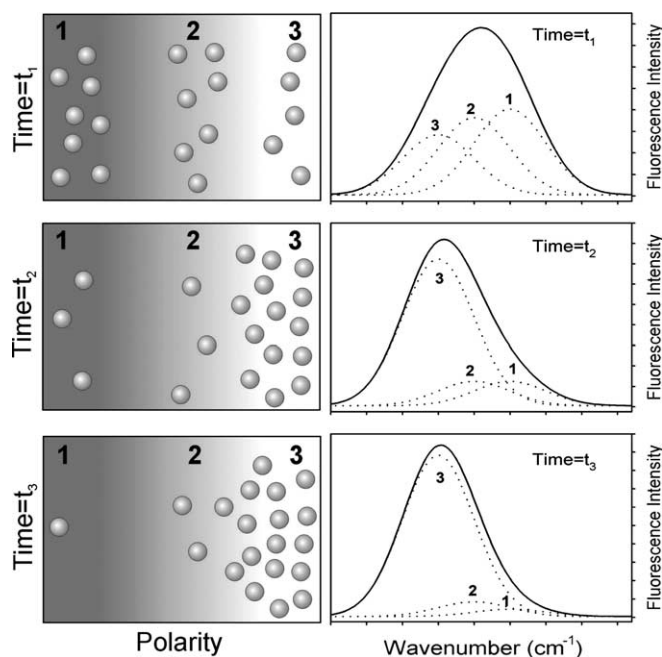


Fig. 3. A schematic representation of the effect of diffusion controlled dynamic heterogeneity on the emission spectrum of a probe at various time-interval after the excitation ($t_1 < t_2 < t_3$). The probe acquires significant dipole moment upon excitation and hence becomes more polar in the excited state. Left panel indicates the population of the probe molecules in three representative environments with different polarities (environment-1 < environment-2 < environment-3) at various times. As time progresses the population of the excited polar probe molecules diffuse to the environment-3. The fluorescence intensity of the spectra (dotted line) as indicated by number 1, 2 and 3 represents population of the probe molecules in the environments 1, 2 and 3 respectively. The solid line is the convolution of the three representative spectra. Note the decrease in fluorescence line-width of the convoluted spectrum, which in turn reflect the temporal diffusion of the probe molecules.

emission spectrum at a particular time ($t = t_1$) would be convolution of the fluorescence spectra of the probe molecules in various environments. The full width at half maximum (FWHM, $\Gamma(t)$) of individual spectrum (line-width) in a particular environment is lower than that of the overall emission spectrum.

Upon excitation, induced dipole moments in the probes make them relatively polar increasing their affinity toward the polar environment-3. As shown in the middle and lower panels of Fig. 3 the population in the environment-3 increases as time progresses. It is evident from Fig. 3 that the translational diffusion of the probe molecules toward the polar environment expectedly decreases the line-width of TRES of the probe molecules. In the case of pure solvation (in absence of diffusion through multiple media and excited state vibrational relaxation) of a ligand in an environment the line-widths of TRES remain same [17]. Similarly, any static heterogeneity (no probe diffusion) will not show any change in line-widths of the TRES.

3. Results and discussion

3.1. Steady-state spectroscopic studies

The solubility (μM) of DCM with the CTAB concentration (mM) as measured from optical density is shown in

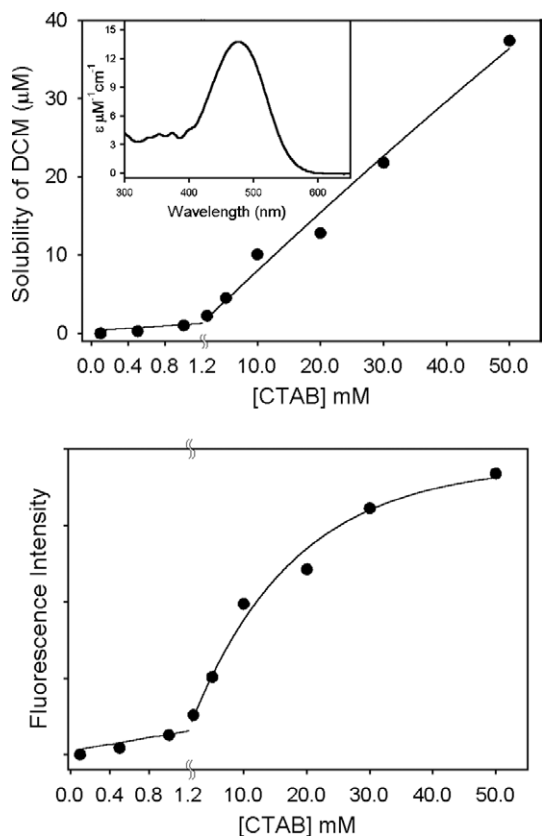


Fig. 4. Upper. Solubility of DCM (μM) vs CTAB concentration (mM). Inset shows extinction coefficient (ϵ) of DCM in 50 mM CTAB. Lower. Plot of normalized fluorescence of DCM in various CTAB concentrations.

Fig. 4. Inset shows absorption spectrum of the probe DCM in 50 mM CTAB solution. From the plot it is evident that below critical micellar concentration (CMC) of CTAB in aqueous solution (~ 1 mM), DCM solubilization is negligible. The observed value of CMC is in agreement with that reported in the literature [19]. The ratio of DCM to micelle is 1:26, which is estimated from the slope of the curve (7.3×10^{-4}) and on taking aggregation constant of CTAB to be 52 [20]. In the lower panel of Fig. 4 we show relative fluorescence intensity of DCM with CTAB concentration in the aqueous solution. The CMC of CTAB (~ 1 mM) and saturation of the fluorescence at higher DCM concentration are evident from the curve. We also studied the solubility of DCM in the enzyme solution (data not shown) and found no solubilization of DCM in absence of the micelle. Above steady-state studies clearly indicate that DCM only makes complex with the micelle and is perfectly suitable to probe the micellar environment even in the presence of CHT in the complex.

Fig. 5 shows absorption and emission spectra of DCM in various systems. The arrow in the absorption spectrum indicates the probe excitation wavelength (405 nm) used in our studies. The fluorescence spectrum in *n*-heptane (nonpolar solvent) has lot of features. The emission spectrum is broad giving a global peak at 530 nm along with two shoulders at 494 nm and 568 nm. In contrast, the emissions of DCM in the micelle and in the enzyme-micelle complex are quite featureless giving peaks at 636 nm and 627 nm respectively. Both of these peaks are significantly red shifted compared to that of the global peak in *n*-heptane at 530 nm. From the emission spectra of DCM in the micelle and in the enzyme-micelle complex it is also evident that a significant population of DCM in the complex face more nonpolar environment compared to that in the micelle without CHT.

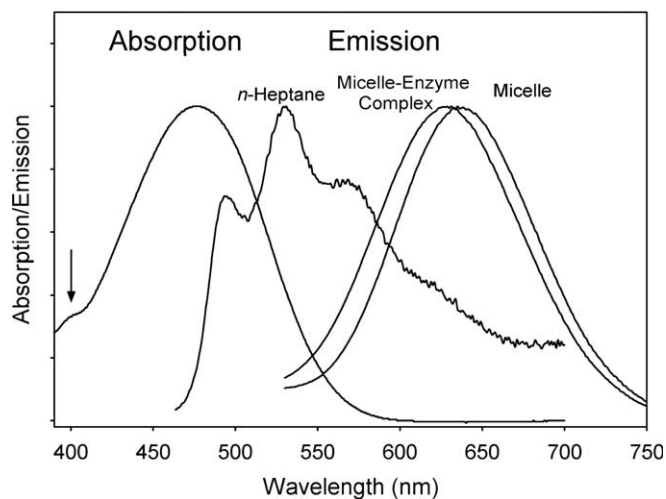


Fig. 5. Steady-state emission spectra of DCM in various environments. The absorption spectrum of DCM in the CTAB micelle is also shown. The arrow indicates the wavelength of excitation (405 nm).

3.2. Time-resolved studies

3.2.1. Location of DCM in the micelle

In a micellar solution, there are three possible locations of the probe (DCM), e.g. bulk water, inner hydrocarbon core and the peripheral stern layer (at the surface). DCM is completely insoluble in water and hence the first possibility can be ruled out. In the hydrocarbon core the emission maximum is expected to be similar to that in *n*-heptane (nonpolar), which is not the case here. Another observation is the dramatic lengthening of excited state lifetime of DCM in the micelle compared to that in *n*-heptane as shown in Fig. 6. The lifetime of DCM in *n*-heptane is found to be less than 50 ps, which is close to the IRF of our instrument and evidently much shorter than that in the micelle (1.8 ns). Moreover DCM molecules staying in the non-polar hydrocarbon core of the micelle is not expected to contribute to the observed solvation dynamics (see below). Thus the emission is exclusively due to the DCM molecules at the surface of the micelle (stern layer).

3.2.2. Solvation dynamics at the surface of the micelle

The dynamics of solvation of the probe ligand (DCM) is reflective of the relaxation of solvent molecules around the excited DCM (Fig. 2). The transients observed at three characteristic wavelengths, from the blue to the red side of the fluorescence spectrum of DCM in the micelle, are

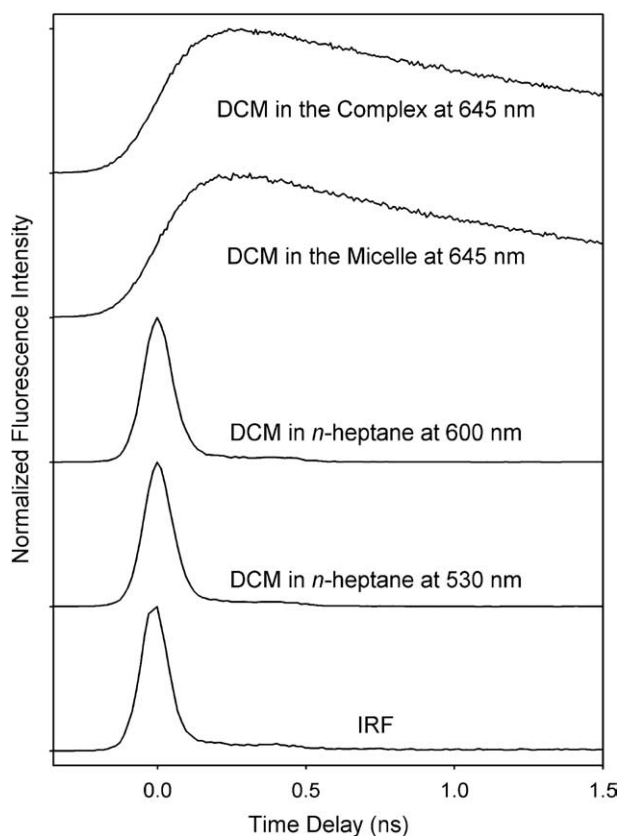


Fig. 6. Normalized fluorescence transients of DCM in various environments. The Instrument response function (IRF) is shown for comparison (excitation at 405 nm).

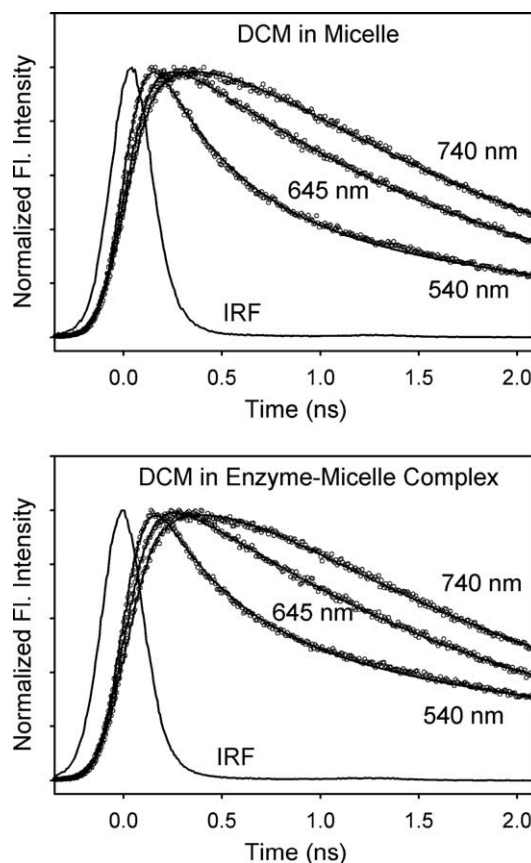


Fig. 7. Time resolved normalized fluorescence transients of DCM in the micelle at 50 mM CTAB concentration in absence (upper) and presence (lower) of the enzyme CHT at three characteristic wavelengths. The instrument response function (IRF) is shown for comparison (excitation at 405 nm).

shown in Fig. 7, upper. The emission transients detected in the blue region (~ 540 nm) of the fluorescence spectrum are characterized by an instant rise (instrument response function, IRF) and a picosecond decay component (~ 400 ps). When detection is done in the red region (~ 740 nm), the decay part slows down until eventually an initial rise on a picosecond time scale (~ 350 ps) is observed. A nanosecond decay component (1.8 ns), which is present at all wavelengths with different contributions, is the lifetime of DCM in the relaxed equilibrium state. These overall features are well recognized as being characteristics of solvation dynamics [11–14,17].

Fig. 8, upper depicts the TRES curves of the probe DCM in the micelle at 50 mM CTAB concentration. The steady-state fluorescence spectrum is shown (dotted line) for comparison with the infinite time (3 ns in this case) spectrum. The time evolution of $C(t)$ is shown in Fig. 9, upper. The results are given in Table 1. The decay curve of the $C(t)$ was fitted to a biexponential function, giving a time constants of 200 ps (52%) and 1.02 ns (48%) where the 50 ps or less component was not resolved. The net dynamical spectral shift is 508 cm^{-1} (from $15,926\text{ cm}^{-1}$ to $15,418\text{ cm}^{-1}$) over a time span of 3 ns. The temporal behavior of the $C(t)$ is very similar to the dynamics observed

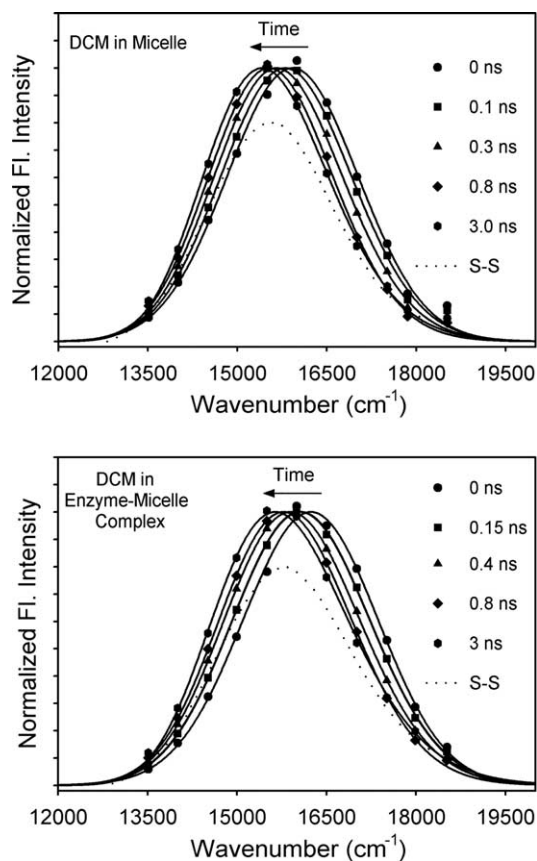


Fig. 8. Time resolved emission spectra (TRES) of the micelle-bound DCM at 50 mM CTAB concentration in absence (upper) and presence (lower) of the enzyme CHT. The dotted curves indicate steady-state emission spectra of DCM in the corresponding sample solutions.

recently using the same probe [13] with excitation wavelength at 300 nm. The study [13] reported a biexponential nature of the decay of $C(t)$ with time constants 170 ps (50%) and 630 ps (50%); estimated average solvation time and net spectral shift were found to be 400 ps and 550 cm^{-1} respectively, consistent with our observations.

To study the degree of orientational rigidity of the probe DCM in the micelle, we obtained the fluorescence anisotropy decay at 645 nm for the excitation wavelength of 405 nm. The $r(t)$ function is the sum of two exponentials (inset of Fig. 9, upper and Table 1) with time constants 873 ps (47%) and 6.7 ns (53%) with $r(t) = 0.32$ at $t = 0$ ns. The faster time constant (873 ps, 47%) may represent local tumbling motion of DCM at the micellar surface. The longer time constant (6.7 ns, 53%) could have relevance to the global motion of the micelle as a whole.

3.2.3. Solvation dynamics of the enzyme-micelle complex

In order to explore the effect of spatial heterogeneity and to investigate change in solvent relaxation at the surface of DCM-labeled micelle upon complexation with CHT, we studied solvation dynamics of the enzyme-micelle complex. Fig. 7, lower shows picosecond-resolved transients of the DCM-labeled micelle-CHT complex in aqueous buffer solution. On the blue edge of the fluorescence spectrum

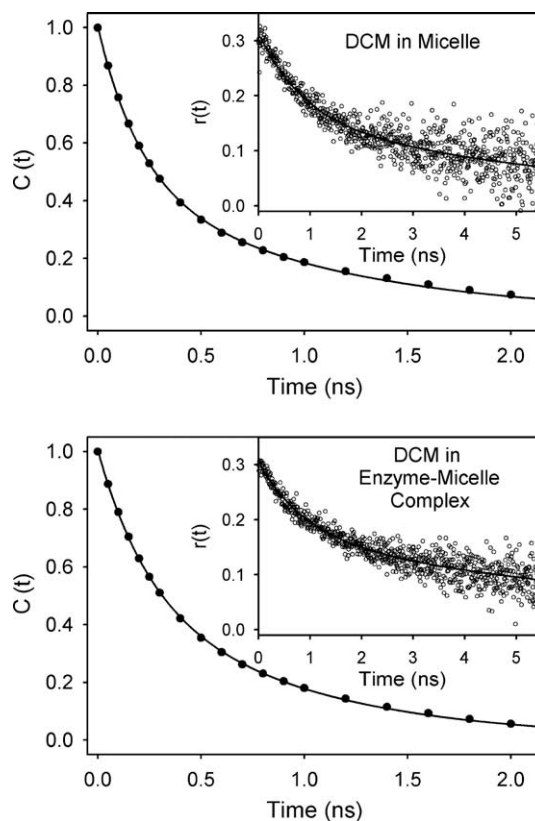


Fig. 9. Solvation correlation function, $C(t)$ of the micelle-bound DCM in absence (upper) and presence (lower) of the enzyme CHT. Insets show time resolved anisotropy, $r(t)$ of DCM in the corresponding samples.

the signals decay with time constants (~ 420 ps), whereas on the red edge the signals are seen to rise (time constant up to 360 ps). A decay component of time constant 1.8 ns reflective of lifetime of the probe is present in all wavelengths detected. Fig. 8, lower shows TRES (up to 3 ns) of the DCM-labeled complex in aqueous buffer. The dotted spectrum indicates the steady-state spectrum of the complex.

The $C(t)$ function in Fig. 9, lower can be fitted to a biexponential decay with time constants of 230 ps (45%) and 870 ps (55%); any sub-50 ps components in these dynamics are unresolved. The net spectral shift is 597 cm^{-1} from 16239 cm^{-1} to 15642 cm^{-1} (up to 3 ns), which is similar to that of the micelle without CHT (Table 1). As shown in the inset of Fig. 9 (lower) the fluorescence anisotropy $r(t)$ at 645 nm decays exponentially to almost baseline with time constants of 910 ps (43%) and 8.7 ns (67%). The value of $r(t)$ at $t = 0$ is found to be 0.3. The faster and slower time constants of $r(t)$ may have relevance to the local tumbling motion and global micellar rotation respectively.

3.2.4. Intermicellar diffusion of DCM: deligation and ligation dynamics

The probe DCM is hydrophobic in the absence of laser excitation. However, upon excitation a significant dipole moment (26.3 D) [21] in the molecule makes DCM polar. In the excited state DCM molecules in a

Table 1

The results of the time dependent solvation and anisotropy measurements of the probe DCM in various environments

Sample	Fluorescence maximum (nm)	Solvation correlation function, $C(t)$	Rotational anisotropy, $r(t)$
DCM in micelle (50 mM CTAB)	636	$\Delta\nu = 508 \text{ cm}^{-1}$ $\tau_1 = 0.20 \text{ ns}, A_1 = 52\%$ $\tau_2 = 1.02 \text{ ns}, A_2 = 48\%$	$r_0 = 0.32$ $\tau_1 = 0.87 \text{ ns}, A_1 = 47\%$ $\tau_2 = 6.70 \text{ ns}, A_2 = 53\%$
DCM in CHT-micelle complex (50 mM CTAB)	627	$\Delta\nu = 597 \text{ cm}^{-1}$ $\tau_1 = 0.23 \text{ ns}, A_1 = 45\%$ $\tau_2 = 0.87 \text{ ns}, A_2 = 55\%$	$r_0 = 0.30$ $\tau_1 = 0.91 \text{ ns}, A_1 = 43\%$ $\tau_2 = 8.70 \text{ ns}, A_2 = 67\%$
DCM in micelle (2 mM CTAB)	636	$\Delta\nu = 486 \text{ cm}^{-1}$ $\tau_1 = 0.18 \text{ ns}, A_1 = 54\%$ $\tau_2 = 0.77 \text{ ns}, A_2 = 46\%$	$r_0 = 0.33$ $\tau_1 = 0.75 \text{ ns}, A_1 = 48\%$ $\tau_2 = 5.13 \text{ ns}, A_2 = 52\%$

microheterogeneous environment (micellar surface) with various polarities would expectedly try to move towards more polar environment (bulk water) making overall environment of the probe molecules to be more homogeneous compared to that in the ground state (Fig. 3). Thus relatively broader fluorescence line-width of DCM immediately after the excitation (almost ground-state configuration) reflecting microheterogeneous environments of the probe molecules decreases with time. In other words, upon excitation, the DCM-labeled micelle undergoes deligation process as the excited DCM comes out of the micellar surface in order to diffuse to a more polar environment. Our depiction of diffusion of DCM and its consequences in the TRES (Fig. 3) is consistent with earlier report [14]. As described in the previous work [17] the role of vibrational relaxation/redistribution of the probe DCM in the temporal behavior of the line-width would be negligibly small. The intramolecular vibrational relaxation/redistribution occurs in these large probe molecules (e.g. DCM) on sub-picosecond time scale [22].

The time dependence of the fluorescence line width ($\Gamma(t)$) of DCM at the micellar surface and in the enzyme-micelle complex at 50 mM CTAB concentration shows interesting dynamics as demonstrated in Fig. 10. For both the samples $\Gamma(t)$ first increases, then decreases and finally increases again with much slower time scale. The time resolved data were fitted numerically by using following multiexponential function, $y = y_0 - A_1 \exp(-t/\tau_1) + A_2 \exp(-t/\tau_2) - A_3 \exp(-(t - T_0)/\tau_3)$. Here τ_1 and τ_3 represent initial faster and final slower rise time constants with preexponential factors A_1 and A_3 respectively. The decay component has time constant τ_2 with preexponential of A_2 . The numerical fitting parameters for the enzyme-micelle complex and the micelle at 50 mM CTAB concentration are shown in Table 2.

The time constants of early rise (τ_1) of ~ 100 ps in the 50 mM CTAB micelle and enzyme-micelle complex (Fig. 10) is comparable to the FWHM of the excitation laser pulse. The dynamical behavior may be due to faster rotational/translational motions reflecting additional temporal heterogeneity generated during the process of excitation of DCM molecules in the spatially heterogeneous medium. The decay components (τ_2) of 0.7 ns and 1.2 ns for the micelle and enzyme-micelle complex respectively,

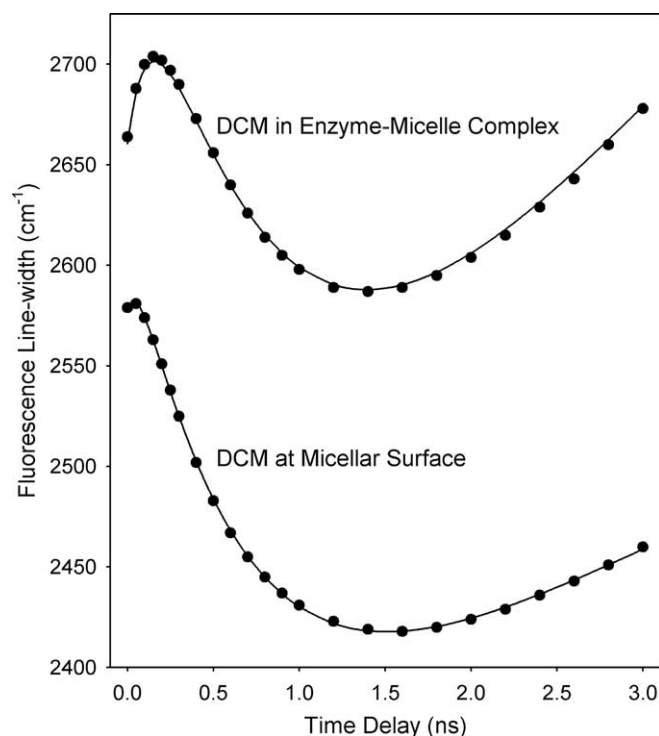


Fig. 10. Full width at half maxima (FWHM, $\Gamma(t)$) of time resolved fluorescence spectra of the micelle-bound DCM at 50 mM CTAB concentration in absence and presence of the enzyme CHT.

which represent restoration of homogeneity in the immediate environments of the probe DCM (see Fig. 3) are consistent with linear diffusion of the probe from a micellar surface toward bulk-water type polar environment. From the dynamical behavior of the probe DCM in the micelle and in the enzyme-micelle complex it is also evident that after 1.4 ns (T_0) of excitation, the probe starts facing heterogeneous environments again revealing increase in $\Gamma(t)$ further. The distance traversed by the probe in 1.4 ns could be estimated as follows. The well-known expression [23] for translational motion in a perpendicular direction of the micellar surface (diffusion in one dimension) is given by, $\tau = d^2/2D$, where τ is the time taken by the probe to cross a layer of thickness d . D is the diffusion constant at the micellar surface. A typical value of D for the CTAB micelle was found to be $15.3 \text{ \AA}^2/\text{ns}$ [19]. The estimated distance traversed by DCM in 1.4 ns is 6.5 \AA . This is similar to the

Table 2
Numerical fitting parameters of the time dependent line-width of DCM emission (50 mM CTAB concentration)

	y_0 (cm ⁻¹)	A_1 (cm ⁻¹)	τ_1 (ns)	A_2 (cm ⁻¹)	τ_2 (ns)	A_3 (cm ⁻¹)	τ_3 (ns)	T_0 (ns)
DCM in micelle	2806	44.3	0.071	338.3	0.70	434	7.64	1.4
DCM in CHT-micelle complex	3123.5	136.4	0.130	857	1.2	802	3.60	1.4

thickness of the stern layer (6–9 Å) of a CTAB micelle, obtained from the structural studies by using small angle neutron scattering experiments [8–10]. Our observation clearly indicates that during the time span of 1.4 ns the probe mostly resides on the stern layer.

The physical origin of the relatively slower rise components (τ_3) of 7.6 ns and 3.6 ns respectively for the micelle and the complex in the $\Gamma(t)$ s after 1.4 ns (T_0) is due to the fact that certain population of the probe molecules that diffuse from the surface of a micelle, enter into the stern layer of another adjacent micelle in the aqueous solution. The diffusion of the probe from bulk type water toward the surface of another micelle expectedly increases the heterogeneity in the immediate environments of the probe DCM resulting increase in $\Gamma(t)$. This observation is not surprising given the fact that at 50 mM CTAB concentration the micelles are closely packed. The micellar concentration at 50 mM CTAB is 0.942 mM on taking aggregation number and CMC of CTAB micelles to be 52 and ~1 mM respectively [20]. Thus the number of micelles in solution is 5.68×10^{23} . By dividing the solution in identical cubes equal to the number of micelles, one can equate the distance between center of the adjacent cubes to the average intermicellar distance, which is found to be 120 Å at 50 mM CTAB concentration. The diameter of the micelle and the thickness of the stern layer were found to be 100 Å and ~10 Å (actually 6–9 Å) respectively from small angle neutron scattering experiment [8–10]. This suggests that adjacent stern layers are negligibly small distance apart at 50 mM CTAB.

A schematic diagram of the micellar packing at 50 mM CTAB concentration is shown in Fig. 11. Note that the probe ligand spends most of its excited state lifetime (1.8 ns) to travel stern layer of a micelle and to enter adjacent layer of another micelle (~1.4 ns). Therefore, upon de-excitation the hydrophobic DCM will be attached to the latter micelle (ligation). The time constant (τ_3) of the rise component of the complex is faster (3.6 ns) than that of the micelle in the absence of the enzyme (7.6 ns). This is consistent with the fact that once the probe gets out of the stern layer of a host micelle, aqueous solution of the complex (mixture of CHT and micelle) would expectedly offers more heterogeneous environments to the probe DCM than that of the micellar solution. Thus the rate of increase of $\Gamma(t)$ for the enzyme-micelle complex would obviously be higher than that of the micelle. The higher heterogeneity of the aqueous solution of the complex than that of the micelle without CHT is also evident from higher y_0 value of the former case (3124 cm⁻¹) than that of the latter one (2806 cm⁻¹).

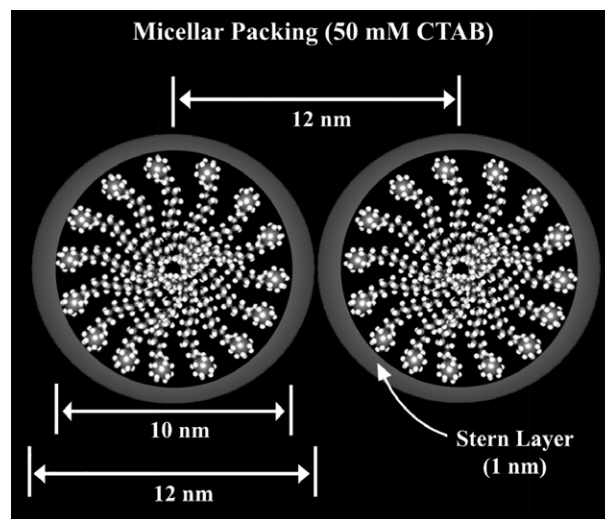


Fig. 11. Schematic diagram showing the micellar packing at 50 mM CTAB concentration.

The dynamical behavior of the probe DCM in the aqueous solution of 2 mM CTAB (CMC ~ 1 mM) further supports above conjectures. The intermicellar distance (center-to-center) at 2 mM CTAB is found to be 416 Å. The solvation correlation function in Fig. 12, upper, can be fitted to a bi-exponential decay with time constants of 182 ps (54%) and 768 ps (46%); any sub-50 ps components in these dynamics are unresolved. Estimated average solvation time and the net spectral shift are 451 ps and 486 cm⁻¹ respectively. The anisotropy $r(t)$ at 645 nm is the sum of two exponentials (inset of Fig. 12, upper) with time constants 0.75 ns (48%) and 5.13 ns (52%) with $r(t) = 0.33$ at $t = 0$. The temporal solvation and anisotropy behavior are similar to those of DCM in 50 mM CTAB solution. The observations suggest that local solvent environment and geometrical restriction of DCM do not change appreciably, upon lowering the concentration of micelles, which in turn increases intermicellar distance.

However, the temporal behavior of the fluorescence line-width ($\Gamma(t)$) at low CTAB concentration (2 mM) is significantly different from that of the higher concentration (50 mM) as shown in the lower panel of Fig. 12. $\Gamma(t)$ shows bi-exponential decay (model: $y = y_0 + A_1 \exp(-t/\tau_1) + A_2 \exp(-t/\tau_2)$) with time constants 125 ps and 741 ps. Note that the longer decay constant (0.74 ns) is comparable to τ_2 value of $\Gamma(t)$ in the micelle at 50 mM CTAB concentration (0.7 ns). No rise components are found in the dynamics of $\Gamma(t)$. The absence of slower rise component (τ_3) observed in the higher micellar concentration is particularly remarkable in this case, which indicates that ligand probe is unable

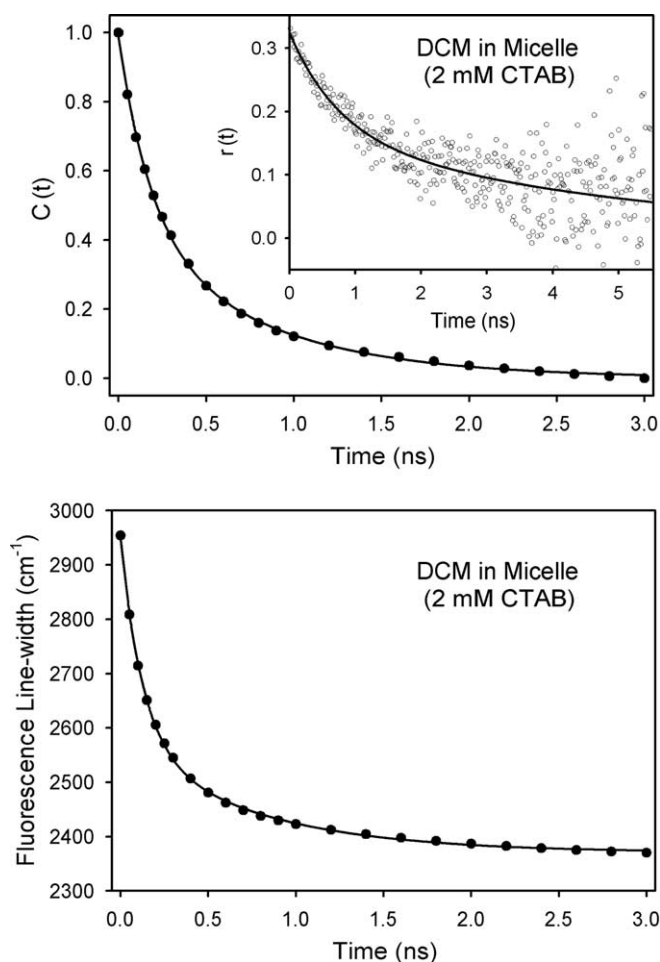


Fig. 12. Upper. Solvation correlation function, $C(t)$ of the micelle-bound DCM at 2 mM CTAB concentration. Inset shows time resolved anisotropy, $r(t)$ of DCM in the sample. Lower. Full width at half maxima (FWHM, $\Gamma(t)$) of time resolved fluorescence spectra of the micelle-bound DCM at 2 mM CTAB concentration.

to ligate a neighboring micelle. This observation is not surprising given the fact that the distance between adjacent layers at 2 mM CTAB concentration is 296 Å offering enough bulk water type intermicellar polar space for the accumulation of the excited DCM molecules. The missing rise at 2 mM CTAB concentration also indicates that the slower growth after 1.4 ns of excitation of the probe DCM in the dynamics of $\Gamma(t)$ is not due to diffusion (in the backward direction) of the ligand to the same micelle (re-ligation) from where it starts diffusing at the beginning. The residual of $\Gamma(t)$ in longer time (3 ns) in this case (2370 cm^{-1}) is relatively lower reflecting lesser spatial heterogeneity compared to that of the micelle (2806 cm^{-1}) and the enzyme-micelle complex (3124 cm^{-1}) at 50 mM CTAB concentration.

4. Conclusion

Studies of picosecond resolved dynamics of the probe DCM in the enzyme-micelle complex elucidate the key time scales involved in solvation, rigidity and ligand diffusion in

the CTAB micelle with and without the enzyme CHT. These studies attempt to link dynamical features for insight into the intercellular communication at various concentration of communicating cells and the enzymatic activity of CHT upon complexation with the micelle.

The solvation dynamics of the enzyme-micelle complex is measured using time dependent Stokes shift of the fluorescence of DCM in the complex. The solvation correlation function ($C(t)$) of the enzyme-micelle complex was found to decay biexponentially with time constants 230 ps (45%) and 870 ps (55%). This dynamical behavior is not much different from the $C(t)$ of micelle-bound DCM without CHT, which also shows biexponential decay with time constant 200 ps (52%) and 1.02 ns (48%). The rigidity of the enzyme-micelle complex is measured using time-resolved anisotropy $r(t)$, which probes orientational motions of the probe DCM adducted to the micelle. The dynamical decay of $r(t)$ of the probe DCM in the enzyme-micelle complex (time constants 910 ps (43%), 8.7 ns (67%)) is not significantly different from that in the micelle alone (time constants 873 ps (47%), 6.7 ns (53%)). Similarities of the solvation and rotational relaxations of the DCM in the enzyme-micelle complex to that of the micelle without the enzyme could be due to the fact that a significant population of DCM does not reside at the interface of the complex. In a recent study [16] we showed that about 35% of the enzyme and micellar surfaces were involved in the complexation. The diameter of the CTAB micelle is comparable to that of CHT (44 Å) [24]. Thus our observations are not surprising given the fact that 65% of the micellar surface is not affected by the complexation with structural intactness of the micelle.

Fluorescence line-width analysis of the enzyme-micelle complex and the micelle without CHT provide us some interesting results. A decay component in the temporal behavior of $\Gamma(t)$ reveals deligation dynamics of the DCM-labeled micelle. The decay component (τ_2) in the case of the enzyme-micelle complex is slower (1.2 ns) compared to that of the aqueous micellar solution (0.7 ns) indicating retarded diffusion (deligation) of the probe in the former restricted environment. In both of the cases relatively slower rise in $\Gamma(t)$ starts after 1.4 ns of excitation of the probe DCM. The distance traveled by the probe from the surface of a host micelle toward the bulk water in 1.4 ns is estimated to be 6.5 Å, which is similar to the thickness of stern layer of the CTAB micelle [8–10]. Thus the residence time of the probe molecule in the stern layer is 1.4 ns. In the micellar solution, as the probe traverses further (after 1.4 ns of excitation) a rise component of 7.6 ns appears in the $\Gamma(t)$ reflecting re-entrance of the probe to the stern layer of adjacent micelle (ligation). The time constants (τ_2 and τ_3) of deligation and ligation dynamics are important for the understanding of ligand mediated intercellular communication. Our studies on the probe DCM at 2 mM CTAB concentration where intermicellar distance 416 Å is much higher than that at 50 mM CTAB (120 Å), distinctly show that the excited DCM is deligated from a

micellar surface but unable to ligate adjacent micelle. Thus the intermicellar communication is completely disrupted at 2 mM CTAB concentration.

From our studies it has been revealed that the diffusion of the probe in the enzyme-micelle complex and in the micelle without CHT is found to be retarded significantly compared to that in free buffer. This observation is also important to understand the catalytic activity of the enzyme in the enzyme-micelle complex. Recently we reported enzymatic activity of CHT upon complexation with the micelle and found to be 7 times retarded compared to that of the enzyme in the free buffer [16]. It was observed that turnover rate, k_{cat} was more affected than the substrate-CHT dissociation constant K_m upon the complexation of CHT with the micelle. As k_{cat} of the enzymatic reaction is expected to depend heavily on the dissociation of the product from the micelle-bound enzyme, slower diffusion of the product is important parameter for the retarded enzymatic activities. Note that in the free buffer a typical time constant of diffusion of an organic molecule (e.g. the product molecule) is much faster (diffusion constant $50 \text{ \AA}^2/\text{ps}$ [25]) than that in micellar environment (diffusion constant $15 \text{ \AA}^2/\text{ns}$ [19]). Our observation of slower probe diffusion in the enzyme-micelle complex as evidenced by τ_2 of $I(t)$ may have implications to the enzymatic activity of α -chymotrypsin upon complexation with the CTAB micelle. Theoretical studies aided by molecular dynamics simulations will be part of our future effort.

Acknowledgements

We thank Dr. Anindya Datta, IITB, India for support and help during the time-resolved measurements. UGC is also thanked for providing fellowship to R.S. and A.K.S.

References

- [1] G.M. Edelman, *Topobiology: An Introduction to Molecular Embryology*, Harper Collins, New York, 1988.
- [2] D.A. Lauffenburger, A.F. Horwitz, Cell migration: a physically integrated molecular process, *Cell* 84 (1996) 359–369.
- [3] K. Francis, B.O. Palsson, Effective intercellular communication distances are determined by the relative time constants for cyto/chemokine secretion and diffusion, *Proc. Natl. Acad. Sci. USA* 94 (1997) 12258–12262.
- [4] Y. Lee, L.V. McIntire, K. Zygourakis, Analysis of endothelial cell locomotion: differential effects of motility and contact inhibition, *Biotechnol. Bioengineer.* 43 (1994) 622.
- [5] M. Pribyl, C.B. Muratov, S.Y. Shvartsman, Discrete models of autocrine cell communication in epithelial layers, *Biophys. J.* 84 (2003) 3624–3635.
- [6] V. Doraiswamy, J. Parrot, M. Skinner, Expression and action of transforming growth factor alpha in normal ovarian surface epithelium and ovarian cancer, *Biol. Reprod.* 63 (2000) 789.
- [7] A. Patist, J.R. Kanicky, P.K. Shukla, D.O. Shah, Importance of micellar kinetics in relation to technological processes, *J. Colloid Interface Sci.* 245 (2002) 1–15.
- [8] S.S. Berr, E. Caponetti, J.S. Johnson, R.R.M. Jones, L.J. Magid, Small angle neutron scattering from hexadecyltrimethylammonium bromide micelles in aqueous solutions, *J. Phys. Chem.* 90 (1986) 5766–5770.
- [9] S.S. Berr, M.J. Coleman, R.R.M. Jones, J.S. Johnson, Small-angle neutron scattering study of the structural effects of substitution of tetramethylammonium for sodium as the counterion in dodecyl sulfate micelles, *J. Phys. Chem.* 90 (1986) 6492–6499.
- [10] S.S. Berr, Solvent isotope effects on alkyltrimethylammonium bromide micelles as a function of alkyl chain length, *J. Phys. Chem.* 91 (1986) 4760–4765.
- [11] H. Zhang, A.M. Jonkman, P. Van der Meulen, M. Glasbeek, Femtosecond studies of charge separation in photo-excited DCM in liquid solution, *Chem. Phys. Lett.* 224 (1994) 551.
- [12] P. Van der Meulen, H. Zhang, A.M. Jonkman, M. Glasbeek, Subpicosecond solvation relaxation of 4-(dicyanomethylene)-2-methyl-6-(*p*-(dimethylamino)styryl)-4H-pyran in polar liquids, *J. Phys. Chem.* 100 (1996) 5367–5373.
- [13] S.K. Pal, D. Sukul, D. Mandal, S. Sen, K. Bhattacharyya, Solvation dynamics of DCM in micelles, *Chem. Phys. Lett.* 327 (2000) 91–96.
- [14] P. Dutta, P. Sen, S. Mukherjee, K. Bhattacharyya, Solvation dynamics in DMPC vesicle in the presence of a protein, *Chem. Phys. Lett.* 382 (2003) 426–433.
- [15] M. Celej, M.S. D'Adrea, P.T.G. Campana, G.D. Fidelio, M.L. Bianconi, Superactivity and conformational changes on α -chymotrypsin upon interfacial binding to a cationic micelles, *Biochem. J.* 378 (2004) 1069.
- [16] R. Sarkar, M. Ghosh, A.K. Shaw, S.K. Pal, Ultrafast relaxation dynamics of a biologically relevant probe dansyl at the micellar surface, *J. Photochem. Photobiol. B: Biol.* 79 (2005) 67–68.
- [17] M.L. Horng, J.A. Gardecki, A. Papazyan, M. Maroncelli, Subpicosecond measurements of polar solvation dynamics: Coumarin 153 revisited, *J. Phys. Chem.* 99 (1995) 17311–17337.
- [18] D.V. O'Connor, D. Phillips, *Time Correlated Single Photon Counting*, Academic Press, London, 1984.
- [19] H.L. Tavernier, F. Laine, M.D. Fayer, Photoinduced intermolecular electron transfer in micelles: dielectric and structural properties of micelle headgroup regions, *J. Phys. Chem. A* 105 (2001) 8944–8957.
- [20] X.-G. Lei, G.-H. Zhao, Y.-C. Liu, N.J. Turro, Influence of binding strength of added electrolytes on the properties of micelles and of micellized radical pairs, *Langmuir* 8 (1992) 475–480.
- [21] M. Meyer, J.C. Mialocq, Ground state and singlet excited state of laser dye DCM: dipolemoments and solvent induced spectral shifts, *Opt. Commun.* 64 (1987) 264.
- [22] T. Elsasser, W. Kaiser, Vibrational and vibronic relaxation of large polyatomic molecules in liquids, *Annu. Rev. Phys. Chem.* 42 (1991) 83.
- [23] S.K. Pal, J. Peon, B. Bagchi, A.H. Zewail, Biological water: femtosecond dynamics of a macromolecular hydration, *J. Phys. Chem. B* 106 (2002) 12376–12395.
- [24] R. Biswas, S.K. Pal, Caging enzyme function: α -chymotrypsin in reverse micelle, *Chem. Phys. Lett.* 387 (2004) 221–226.
- [25] C.H. Cho, M. Chung, J. Lee, T. Nguyen, S. Singh, M. Vedamuthu, S. Yao, J.-B. Zhu, G.W. Robinson, Time and space resolved studies of the physics and chemistry of liquid water near a biologically relevant interface, *J. Phys. Chem.* 99 (1995) 7806–7812.